Chapter 19
Design of a Tuned Vibration Absorber with Friction Contact for High Location Ratio Application

Matthew W. Hancock, Nathan P. Lovell, Yusuf R. Shehata, Keegan J. Moore, Bogdan I. Epureanu, Thomas N. Thompson, and Sean T. Kelly

Abstract Tuned vibration absorbers (TVAs) are passive devices commonly used to reduce the vibration amplitude of a host structure subject to harmonic excitations. These devices are designed so that vibration energy flows from the host structure to the TVA, which dissipates that energy using linear damping mechanisms. However, devices using nonlinear energy dissipation methods, such as friction-enhanced TVAs, have recently been explored. Additionally, it is desirable to place a TVA on the host structure where large vibration amplitudes occur, but this is often not feasible in practice. The ratio of the amplitudes of a high-vibration-amplitude area to a low-vibration-amplitude area is referred to as the location ratio (LR). Careful tuning of the TVA is critical to ensure effective energy absorption, especially when the TVA is placed in a high-LR area. This paper presents a case study of a novel TVA design that is optimized for high-LR applications and utilizes nonlinear friction contacts to dissipate energy. The host structure analyzed is the Box Assembly (BA), an experimental structure previously analyzed for vibration testing. A finite element model of the BA, validated by experimental ping tests, is considered, and a target mode of the BA is selected for TVA design. Simulations are performed to illustrate the effectiveness of the TVA in a high-LR application by varying linear system parameters. The effects of TVA nonlinear friction damping on the vibration amplitude reduction are also investigated. From these simulations, TVA design considerations are suggested.

Keywords Tuned Vibration Absorber · Friction · Location Ratio · Nonlinear Dynamics · Vibrations

Introduction

Large vibration amplitudes in structures subject to harmonic excitations can increase risk of high cycle fatigue and failure, especially when the structure's operating and natural frequencies coincide. For such systems, vibration suppression is critical

Matthew W. Hancock
Department of Mechanical Engineering, Texas A&M University
e-mail: matthewhancock@tamu.edu

Nathan P. Lovell
Department of Civil and Environmental Engineering, The Catholic University of America
e-mail: nathanplovell@gmail.com

Yusuf R. Shehata
Department of Mechanical and Aerospace Engineering, University of California, San Diego
e-mail: yusufrshehata@gmail.com

Keegan J. Moore
Daniel Guggenheim School of Aerospace Engineering, Georgia Institute of Technology
e-mail: kmoore@gatech.edu

Bogdan I. Epureanu
Department of Mechanical Engineering, University of Michigan, Ann Arbor
e-mail: epureanu@umich.edu

Thomas N. Thompson · Sean T. Kelly
Los Alamos National Laboratory
e-mail: tnthompson@lanl.gov; stkelly@lanl.gov

Ludovic Renson et al. (eds.), *Nonlinear Structures & Systems, Vol. 1*, Conference Proceedings of the Society for Experimental Mechanics Series, https://doi.org/10.13052/97887-438-0146-7_19

to the health of structural components that experience cyclical loading. A common solution for vibration reduction is to introduce a tuned vibration absorber (TVA), a linear, passive device designed to reduce the amplitude of vibration of a host structure subject to harmonic excitation. The TVA (also referred to as a tuned mass damper, or TMD) is tuned to target a specific frequency of interest, usually a natural frequency at which unwanted vibration amplitudes are experienced by the host. TVAs are typically less than 5% of the mass of the host structure [1], and can vary based on the application, placement, and host structure geometry, among other factors. A typical TVA absorbs the host's vibration energy by transferring that energy to an external mass, causing it to oscillate. As a result of this energy transfer, the TVA mass can have a relatively high response amplitude while the host's vibration is reduced.

Because of their ability to effectively mitigate unwanted vibrations, there are a myriad of applications in which TVAs have been applied across civil [1, 2], mechanical [2], and aerospace fields [3–6]. For example, skyscrapers using TVAs include the John Hancock Tower in Boston and the Citicorp Center in Manhattan [1]. In these structures, one or more TVAs are installed on the upper floors of the building to dissipate energy and reduce building response due to wind loads. An example of a mechanical application of TVAs is in pipelines above the arctic circle, in which wind loads and the associated vortex shedding can excite vibration modes of the pipelines [2]. In this example, TVAs have been installed on each span of the pipe to prevent fatigue cracking at the pipe joints. Another example is that presented by Aksoy et al. in which a TVA was designed to reduce vibrations of an air vehicle missile launcher [7]. Being so common, the linear dynamics of TVA-host systems have been studied extensively, and TVA theory is well known [1].

Recently, work has been conducted to increase the effectiveness of TVAs by incorporating nonlinear energy dissipation methods, such as friction [3, 8–12] and impacts [3, 8, 9, 12]. These methods have been shown to provide significant vibration reduction; however, introducing nonlinearity presents additional challenges and computational effort with respect to modeling and tuning to the resonant frequency of interest. In particular, frictional nonlinearities arise from transitions between a "stuck" state, in which there is no relative motion between friction contacts, and a "slip" or "sliding" state, in which contacts are moving freely with respect to each other. As a result, relative to linear TVA dynamics, predicting the response of such designs is more challenging. Many "friction-enhanced" TVA designs have been developed [10–14], with their associated modeling and experimental difficulties having been studied extensively in literature [15, 16]. Despite the additional modeling challenges, introducing nonlinear energy dissipation methods can provide additional vibration reduction in to-be-discussed scenarios where a linear TVA is insufficient.

Another important factor that affects TVA effectiveness is the location at which the TVA is placed on the host structure. It is typically desirable to place a TVA at the location of highest vibration amplitude on the host; this positioning can best facilitate energy flow from the host structure into the TVA to be dissipated. However, in many cases, it is not feasible to place the TVA at these high-amplitude locations, so the TVA must be designed to be effective at a low-amplitude location on the host structure. Location ratio (LR) is a metric that quantifies this amplitude difference, defined as the ratio of the highest vibration amplitude on the host structure to the amplitude at the mounting location of the TVA. This metric has been considered in previous work by Lupini et al. [5] and Mitra et al. [17]. At the location of highest amplitude, the LR is equal to one, and increases as the TVA is moved to areas of lower vibration amplitude. High-LR areas on a structure are areas of relatively low vibration amplitude, meaning less kinetic energy can be transferred to a TVA at this location. An example of a high-LR application is a ring damper designed for a turbomachinery blisk, like that in Refs. [3, 18, 19]. Blisks are rotating, fanlike structures used in modern turbomachinery whose service environment and inherent mistuning (i.e., deviations from nominal geometry and material properties) can create damaging vibration-induced stresses that may lead to high cycle fatigue failure. It is not feasible to mount a TVA at the tips of the blades where the highest vibration amplitude often occurs; doing so would interfere with the fluid flow, and thus lower engine performance. Therefore, it is necessary to mount the TVA in the disk portion of the blisk, where the LR is high. TVAs for this application have been designed and simulated by Lupini et al. [4, 19] and Cimpuieru et al. [3, 8, 9] which have yielded promising results.

Although effective TVA designs have been produced for high-LR applications, even those which include nonlinear energy dissipation methods, these designs primarily target a niche application in their respective field. Given that these designs have proven promising, a flexible, generalized set of design guidelines would be useful in helping designers develop effective friction-enhanced TVAs for other structures. As such, this paper presents a set of design considerations for friction-enhanced TVAs for high-LR placement. This paper describes the design of a friction-enhanced TVA for application on a simple host structure, known as the Box Assembly (BA). First, a brief overview of TVA theory is presented. Second, the process of creating and validating a finite element (FE) model of the BA is described. Third, a directional study considering a single-degree-of-freedom (SDoF) TVA is conducted using a reduced-order model (ROM) of the BA. Fourth, the TVA design process is discussed, and the final TVA design used for the BA is presented. Fifth, multiple BA-TVA systems are simulated with and without including nonlinear friction contacts considering various TVA attachment locations. The paper concludes with a discussion of the simulation results and design considerations that can be drawn from this study.

Methods

This section begins with a discussion of relevant theory concerning host-TVA systems, followed by the methods used for TVA design. First, an FE model of the host structure, i.e., the BA, was created and calibrated using experimental frequency response functions (FRFs) extracted from ping testing. Second, a reduced-order model (ROM) of the BA was created and used for an initial SDoF TVA directional analysis. Third, the TVA was designed and combined with the BA to form multiple BA-TVA FE models considering various TVA attachment locations. Fourth, the BA-TVA combined systems were simulated with and without friction. The results of these simulations informed the tuning of the TVA, making this step iterative. Finally, the results of the simulations with the tuned TVA led to the results and conclusions. This TVA design workflow is portrayed in Fig. 1.

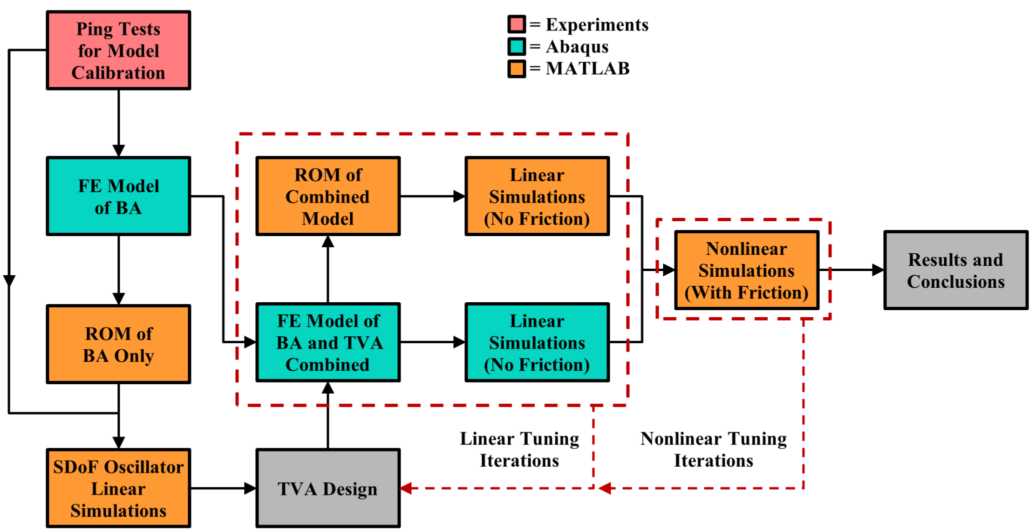

Fig. 1 TVA design workflow.

Theory

The linear equations of motion (EoMs) for a host structure combined with a TVA are given as:

$$\boldsymbol{M}\ddot{\boldsymbol{x}} + \boldsymbol{C}\dot{\boldsymbol{x}} + \boldsymbol{K}\boldsymbol{x} = \boldsymbol{f}_E \tag{1}$$

where $\boldsymbol{f}_E$ is the external forcing vector, $\ddot{\boldsymbol{x}}$, $\dot{\boldsymbol{x}}$, and $\boldsymbol{x}$ are the system response vectors in terms of physical acceleration, velocity, and displacement, respectively, and $\boldsymbol{M}$, $\boldsymbol{C}$, and $\boldsymbol{K}$ are the system mass, damping, and stiffness matrices, respectively. For an elastically coupled host-TVA system, $\boldsymbol{M}$ and $\boldsymbol{K}$ have the general form:

$$\boldsymbol{M} = \begin{bmatrix} \boldsymbol{M}_{host} & 0 \\ 0 & \boldsymbol{M}_{TVA} \end{bmatrix}; \quad \boldsymbol{K} = \begin{bmatrix} \boldsymbol{K}_{host} & \boldsymbol{K}_c \\ \boldsymbol{K}_c^T & \boldsymbol{K}_{TVA} \end{bmatrix} \tag{2}$$

where $\boldsymbol{M}_{host}$ and $\boldsymbol{K}_{host}$ correspond to the host structure alone, $\boldsymbol{M}_{TVA}$ and $\boldsymbol{K}_{TVA}$ the TVA alone, and $\boldsymbol{K}_c$ the linear elastic coupling between host and TVA. For the applications considered in this work, the external forcing is assumed to be harmonic, and can be defined as $\boldsymbol{f}_E = \widehat{\boldsymbol{f}}_E e^{i\omega t}$, where $\widehat{\boldsymbol{f}}_E$ is the complex forcing in the frequency domain, $i = \sqrt{-1}$, ω is the forcing frequency in rad/s, and t is time. Accordingly, for the linear EoMs in Eq. (1), a harmonic input force yields a harmonic response of the form $\boldsymbol{x} = \widehat{\boldsymbol{x}} e^{i\omega t}$, where $\widehat{\boldsymbol{x}}$ is the complex response in the frequency domain. Substituting these terms into Eq. (1) yields the frequency-domain EoMs:

$$\left[-\omega^2 \boldsymbol{M} + i\omega \boldsymbol{C} + \boldsymbol{K}\right] \widehat{\boldsymbol{x}} = \widehat{\boldsymbol{f}}_E \tag{3}$$

For the host structure considered in this work, while the model fidelity is such that Eq. (3) could be solved directly in system coordinates without significant computational cost, when nonlinearities are introduced, these equations become prohibitive to solve. Thus, to reduce computational cost, the system matrices are reduced using Craig-Chang component mode synthesis (CC-CMS) [20] with a Galerkin projection scheme. Reduced mass, damping, and stiffness matrices are denoted as $\widetilde{\boldsymbol{M}}$, $\widetilde{\boldsymbol{C}}$, and $\widetilde{\boldsymbol{K}}$, respectively, along with reduced frequency-domain forcing $\hat{\widetilde{\boldsymbol{f}}}_E$ and responses $\hat{\widetilde{\boldsymbol{x}}}$, where $\hat{\widetilde{\boldsymbol{x}}}$ contains master (i.e., retained) degrees of freedom (DoFs), $\hat{\widetilde{\boldsymbol{x}}}_m$, and secondary DoFs, $\hat{\widetilde{\boldsymbol{x}}}_s$. In addition, damping for this system is approximated using Rayleigh damping, where the damping matrix $\widetilde{\boldsymbol{C}}$ (and $\boldsymbol{C}$) is assumed proportional to the mass matrix such that $\widetilde{\boldsymbol{C}} = \alpha\widetilde{\boldsymbol{M}}$. The Rayleigh damping coefficient α is related to the modal damping ratio, ζ, by Eq. (4):

$$\zeta = \frac{\alpha}{2\omega} \tag{4}$$

For this work, α is assumed to be constant for all frequencies. Using the natural frequency for the host structure's targeted mode (here, the fundamental mode) ω_1 and experimentally measured damping, ζ_{exp}, yields Eq. (5):

$$\alpha = 2\zeta_{exp}\omega_1 \tag{5}$$

Using this definition of $\widetilde{\boldsymbol{C}}$, Eq. (3) can be rewritten in terms of reduced quantities as:

$$\left[\left(-\omega^2 + i\omega\alpha\right)\widetilde{\boldsymbol{M}} + \widetilde{\boldsymbol{K}}\right]\hat{\widetilde{\boldsymbol{x}}} = \hat{\widetilde{\boldsymbol{f}}}_E \tag{6}$$

All linear simulations to follow involve solving Eq. (6) (using MATLAB's mldivide function) considering ω values in a frequency range of interest. When a nonlinear force such as friction is added to the system, an additional term, $\boldsymbol{f}_{NL}$, is included in the system-level EoMs in Eq. (1) to give:

$$\boldsymbol{M}\ddot{\boldsymbol{x}} + \boldsymbol{C}\dot{\boldsymbol{x}} + \boldsymbol{K}\boldsymbol{x} = \boldsymbol{f}_E + \boldsymbol{f}_{NL}(\boldsymbol{x}, \dot{\boldsymbol{x}}) \tag{7}$$

Again, the damping matrix is assumed as $\boldsymbol{C} = \alpha\boldsymbol{M}$. Additionally, CC-CMS is used, where all DoFs at nodes that: 1) have non-zero nonlinear friction contact forces, 2) are response DoFs, and/or 3) have non-zero applied external forces are included in $\boldsymbol{x}_m$. For this work and adopting notation from Ref. [21], it is assumed that the friction force $\boldsymbol{f}_{NL}$ is represented by dry Coulomb friction characterized by a signum function, which is approximated with a hyperbolic tangent function as:

$$\boldsymbol{f}_{NL}\left(\boldsymbol{x}_m, \dot{\boldsymbol{x}}_m\right) \approx \sum_e \boldsymbol{w}_e \mu N \tanh\left(\frac{\dot{x}_{m,e}}{\epsilon}\right) \tag{8}$$

where e is a summation index/identifier for a nonlinear DoF contact pair, $\boldsymbol{w}_e$ is a vector with a single $+1$ and -1 at indices of the contact pair DoFs for nonlinear element e and zeros elsewhere, $\dot{x}_{m,e}$ is the relative velocity between the contact pair e DoFs (always a scalar), and ϵ is a regularization coefficient dictating the sharpness of the hyperbolic tangent function's transition. ϵ can be modified to aid in computation and soften the set of equations, with smaller ϵ yielding closer approximations to the signum function [21]. While μ, N, and ϵ can be chosen to be dependent on e, for this work in which only a single friction contact pair is considered for all nonlinear simulations (i.e., max $e = 1$), this was not applicable. Substituting Eq. (8) into Eq. (7) and using CC-CMS reduced-order quantities yields:

$$\widetilde{\boldsymbol{M}}\ddot{\widetilde{\boldsymbol{x}}} + \alpha\widetilde{\boldsymbol{M}}\dot{\widetilde{\boldsymbol{x}}} + \widetilde{\boldsymbol{K}}\widetilde{\boldsymbol{x}} = \widetilde{\boldsymbol{f}}_E + \sum_e \widetilde{\boldsymbol{w}}_e \mu N \tanh\left(\frac{\dot{\widetilde{x}}_{m,e}}{\epsilon}\right) \tag{9}$$

Note that any non-zero entries in $\widetilde{\boldsymbol{w}}_e$ are associated with master DoFs, with zeros for all secondary DoFs for all e. Similarly, retained DoFs are chosen such that the relative velocity $\dot{\widetilde{x}}_{m,e}$ will only be between master DoFs for all e. The nonlinear simulations to follow involve solving Eq. (9) in the time domain using the first-order, state space form given by:

$$\begin{bmatrix} \dot{\boldsymbol{x}} \\ \dot{\boldsymbol{y}} \end{bmatrix} = \begin{bmatrix} \boldsymbol{y} \\ \widetilde{\boldsymbol{M}}^{-1}\left(\widetilde{\boldsymbol{f}}_E - \widetilde{\boldsymbol{K}}\boldsymbol{x} - \alpha\widetilde{\boldsymbol{M}}\boldsymbol{y} + \sum_e \widetilde{\boldsymbol{w}}_e \mu N \tanh\left(\frac{y_{m,e}}{\epsilon}\right)\right) \end{bmatrix} \tag{10}$$

where $\boldsymbol{x}$ and $\boldsymbol{y}$ in Eq. (10) are general state variables still considering the reduced-order coordinates, and $y_{m,e}$ still represents the relative velocity between the retained DoFs of contact pair e. Because steady-state response amplitudes are sought for all nonlinear FRFs, Eq. (10) is simulated for enough time steps to ensure convergence to a steady-state response for a given ω.

Model Creation and Validation

Before beginning the TVA design process, a model of the host structure, i.e., the BA, was needed. Though previous models of the BA have been created using nominal dimensions [22], it was found that the measured dimensions of the BA considered in this study varied from the nominal. Therefore, the FE model created for this study considered measured dimensions, with significant dimensions shown in Fig. 2. For this work, all high-fidelity models and ROM matrices were created using Abaqus/CAE 2023 software. A mesh convergence study was completed to: 1) ensure modal analysis results (i.e., natural frequencies) were converged, and 2) choose a practical seed size to reduce the computational effort of any high-fidelity simulations and ROM matrix generation. It was determined that a 3 mm seed size using quadratic elements yielding a mode 1 natural frequency of 82.38 Hz was sufficient. Note that this was only for initial model development.

Because TVA effectiveness is highly dependent on the target mode, particularly for a structure with low inherent damping such as the BA, it is critical that the FE model accurately represent the as-manufactured BA with respect to: 1) the target mode's natural frequency and damping, and 2) the FRF response amplitude at and around the targeted mode. For reasons discussed in later sections, mode 1 was chosen as the target mode for this study. As such, identification of the natural frequency and damping of mode 1 was of greatest interest.

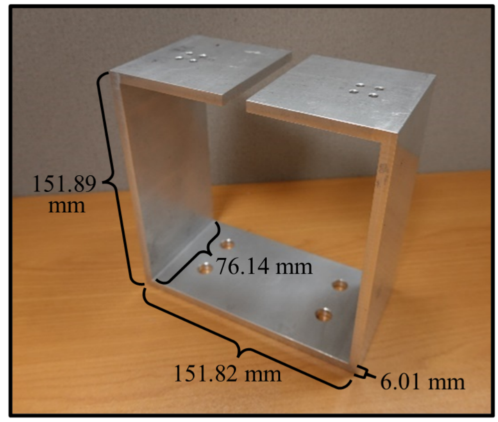

Fig. 2 BA with measured dimensions shown.

A series of ping tests (i.e., impact or hammer tests) were conducted on the BA to experimentally determine the mode 1 damping ratio and first four natural frequencies. For this study, free-free boundaries were considered. Thus, to mitigate any external interference and approximate a free-free boundary condition, the BA was suspended in such a way as to reduce interference and friction at attachment points. As shown in Fig. 3, this low-interference suspension system was achieved using an aluminum box frame, from which fishing line (South Bend M1420 Monofilament Line) connected to rubber bands (Pale Crepe Gold) held the BA aloft in the center of the frame. Fishing line was used to reduce friction at suspension points, and the flexibility of the rubber bands ensured that the tensile forces from the fishing line had a negligible effect on the dynamics of the system.

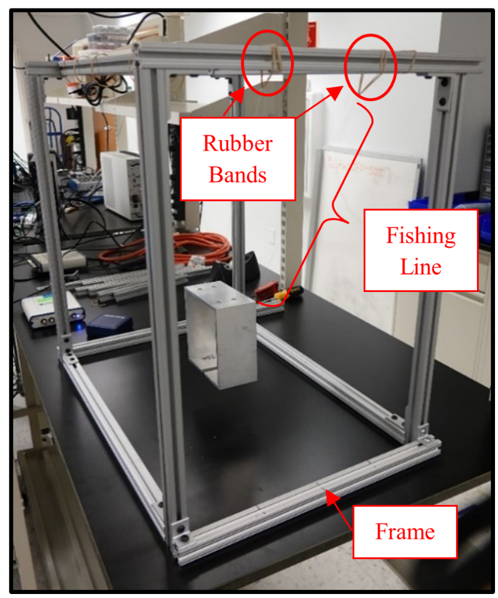

Fig. 3 Ping test experimental setup with BA suspended using rubber bands, fishing line, and an aluminum frame. Accelerometer not shown.

The hammer impact location and the placement location and orientation of a single-axis accelerometer were varied across seven ping tests to test the sensitivity of the BA's response to these variables. Additionally, the angle at which the BA was suspended from the fishing line attachments was varied for this same purpose. It was found that the measured natural frequencies varied negligibly across all hammer impact and accelerometer locations and suspension configurations. The average measured natural frequency of mode 1 was 83.25 Hz, and all measurements were within 0.1% of that value.

Initially, the average measured mode 1 natural frequency differed from the predicted mode 1 natural frequency from the FE model (82.38 Hz) by 0.87 Hz, a 1.05% error. Although this error is appreciably low, due to the BA's low inherent damping, an error of less than 0.50% was desired to consider the model acceptable for this study. Therefore, further model refinement was necessary. Three parameters – Young's modulus, mass density, and geometry – were considered for the purpose of refining the FE model to more closely match the experimentally measured mode 1 natural frequency. Because the mass density and geometry were based on experimental measurements, Young's modulus was modified uniformly across the BA. It was found that increasing the Young's modulus by 1.42% (from 69×10^9 Pa to 70×10^9 Pa) yielded a mode 1 natural frequency of 82.96 Hz, reducing the error to an acceptable 0.35%.

With the model geometry and targeted mode 1 natural frequency calibrated, the final model calibration step was to match the experimental and BA ROM FRFs (ROM details are discussed shortly), specifically around the mode 1 natural frequency. In this work, FRFs are defined as the displacement magnitude of the x-DoF at node 1 divided by the external forcing magnitude (here, the terms magnitude and amplitude are used interchangeably, both referring to the peak-to-peak amplitude divided by 2). Calibrating the ROM FRF was achieved by modifying the mass proportional Rayleigh damping coefficient α, initially estimated as 0.4 rad/s for $\zeta_{exp} \approx 0.0004$ obtained for mode 1 using the half-power method. After reducing α to 0.31 rad/s, the BA ROM FRF magnitude was approximately 0.015 m/N at the mode 1 resonance, corresponding to $\zeta \approx 0.0003$

(or 0.03%). Figure 4 shows strong agreement around the mode 1 natural frequency between the calibrated BA ROM FRF and a representative experimental FRF. While experimental ζ estimates can provide initial estimates of α using Eq. (5), for an isolated target mode like that considered here and for host structures with low inherent damping, small modifications like those done in this work are still likely necessary. Figure 5 shows the shape of mode 1 from the calibrated FE model, which exhibits an opening-closing motion with much of the displacement occurring in the x-y plane.

In summary, after calibration, the three quantities of interest – natural frequency, damping, and FRF magnitude – were in agreement between the experiment and BA ROM for mode 1. It is important to note that while this FE model of the BA may not be valid for other studies, applications, or higher-order modes, this study is only concerned with the behavior of the BA at frequencies at or near the natural frequency of mode 1. Thus, this FE model was considered valid for the purposes of this study.

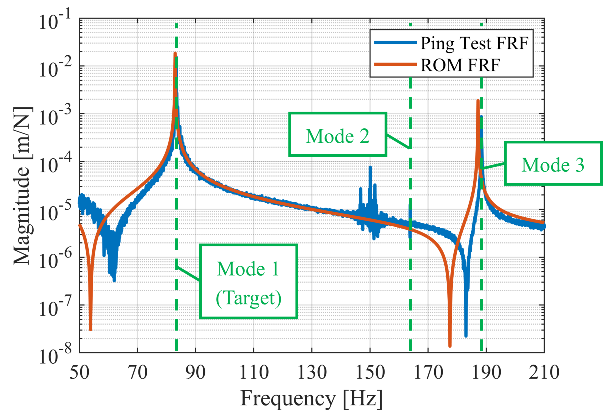

Fig. 4 Comparison of FRFs from the calibrated BA ROM and a representative ping test with first three modes indicated.

For all high-fidelity FE models (with or without a TVA), CC-CMS reduced-order mass and stiffness matrices were generated within Abaqus/CAE and exported to be processed in MATLAB. For the BA alone, master DoFs included all DoFs at all considered TVA placement locations (see Fig. 6). This ROM was used for the model calibration and included 5 retained nodes with 3 translational DoFs each as master DoFs, and 14 secondary (modal) DoFs. The locations of the retained nodes were selected to represent a range of LRs for mode 1 and are shown in Fig. 6. These nodes (node 1 – node 5) are the considered TVA attachment locations and will be referred to throughout the remainder of this work. For combined BA-TVA systems, master DoFs included all DoFs at forcing and response nodes and all DoFs for nodes included in the friction contact.

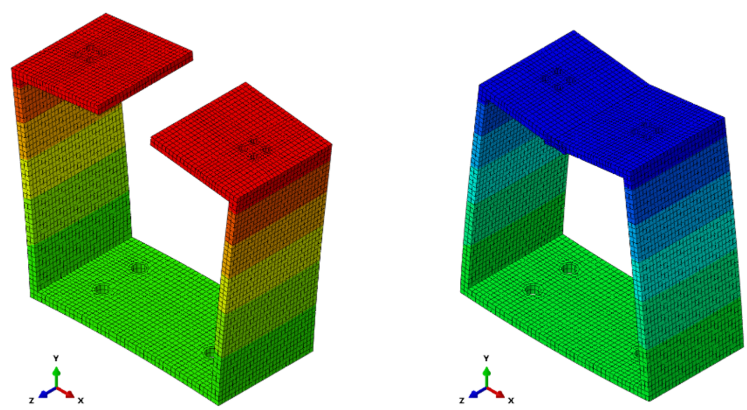

Fig. 5 Mode 1 of calibrated BA FE model. Green represents locations with little to no displacement magnitude, while red and blue represent large positive and negative displacement magnitudes, respectively.

Location Ratio

At a given excitation frequency, the LR for node i is defined in Eq. (11), where the total displacement magnitude at node 1 is divided by the displacement magnitude at node i. Note that the LR can also be calculated using the mode shape alone, which, because mode 1 is significantly isolated from all other modes, is almost identical.

$$\mathrm{LR}_i = \frac{\|\boldsymbol{x}_1\|_2}{\|\boldsymbol{x}_i\|_2} \tag{11}$$

Node 1 was chosen as the reference node for calculating LR because that is where the maximum deflection was observed for the considered harmonic forcing (applied in the x-direction at node 1). The LR of each considered node is shown in Fig. 6.

SDoF TVA Directional Analysis

Before performing any high-fidelity TVA design, a series of linear simulations were conducted to determine the effect of the oscillation direction on TVA effectiveness. Knowing which TVA oscillation direction (at each node) has the greatest effect on host response amplitude can aid design efforts and inform understanding of the energy transfer from the host structure. For these simulations, the reduced-order mass and stiffness matrices were augmented to be of the form shown in Eq. (2) by independently including a SDoF oscillator along each DoF for all nodes shown in Fig. 6, yielding 15 BA-SDoF-TVA systems (5 nodes with 3 DoFs each). These augmented mass and stiffness matrices were used to compute linear FRFs for each BA-SDoF-TVA system. This allowed for the study of linear TVA effectiveness across different TVA placements and orientations with a simple, computationally efficient system.

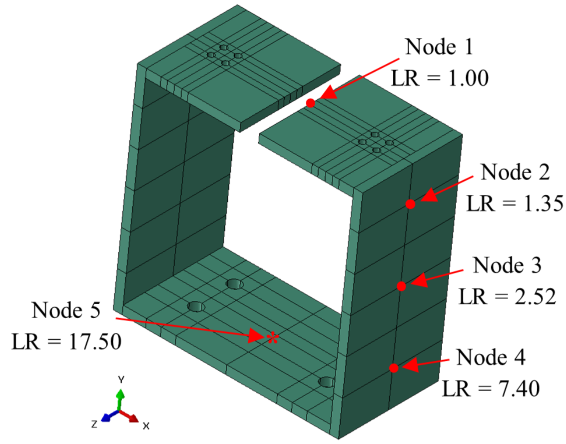

Fig. 6 The 5 nodes considered for TVA placement with respective location ratios (* indicates node on backside relative to view shown).

Because the TVA is modeled as a base-excited SDoF oscillator, it is most excited when the base vibrates in the same direction as the oscillator (i.e., when the SDoF TVA direction and predominant host motion at the attachment location are aligned). Considering a harmonic forcing excitation in the x-direction at node 1, Fig. 7 shows the effect of changing the SDoF TVA's oscillation direction on the peak magnitude reduction of the BA FRF when targeting mode 1 (response reduction is considered for the x-DoF FRF at node 1). Peak magnitude reduction refers to the percent decrease in maximum magnitude across all frequencies in the FRF. The frequency range considered for calculating quantities in Fig. 7 was 65 to 105 Hz. It can be seen in Fig. 7 that a TVA aligned in the x-direction has the greatest reduction at nodes 1 – 4, but alignment in the y-direction has the greatest reduction at node 5. Based on the mode shape in Fig. 5 (and because this mode is isolated as shown in Fig. 4), these results are intuitive given that the forced response deflection shape in this frequency range will be significantly dominated by mode 1. However, for a host structure with a more complex dynamic response, this may not be as evident, and performing this initial study provides a quantitative estimate of TVA directional effectiveness to inform the design process. Additionally, one may consider a local coordinate system that better aligns with dominate motions at candidate nodes.

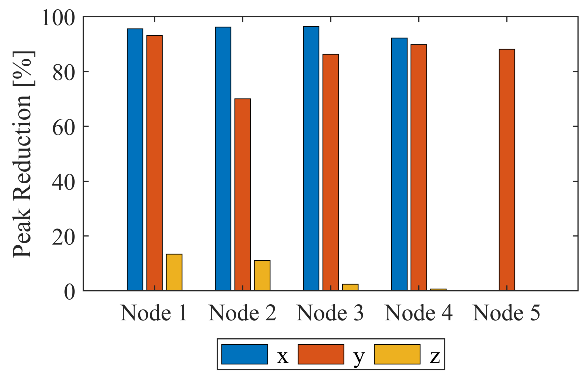

Fig. 7 Effect of SDoF TVA oscillation direction at each considered node on BA peak reduction.

One can also include a friction contact between the BA and SDoF TVA to study the effect of friction on SDoF TVA performance as a function of location and orientation. Though nonlinear analyses for BA-SDoF-TVA systems are not shown for brevity, such simulations can be useful to provide an estimate of nonlinear effectiveness.

TVA Design

To conduct the presented linear and nonlinear parametric studies, a novel TVA for the BA was designed. The TVA had to meet several criteria to be applicable for this study including: 1) a dominant oscillation direction, 2) predictable oscillatory behavior, 3) ease of manufacturing and repairability, 4) a predictable point of friction contact, and 5) tunability with respect to linear and nonlinear behavior. This section discusses the latter portions of the workflow presented in Fig. 1, particularly the iterative TVA design process. Included are notes of design concepts that were not selected for the final model but may be of interest when designing for different host structures and applications. For reference, Fig. 8a displays the detailed model of the TVA design. For the purpose of focusing this study's scope to nonlinear friction contact effects, this model was defeatured, as shown in Fig. 8b, and potential complexities due to nonlinear geometric and fastener physics ignored.

The first design aspect considered was the mechanical apparatus used for oscillation. Apparatuses considered include strings, a cylindrical cantilever beam, a mass-loaded spring, and a rectangular fixed-fixed flexure. The rectangular fixed-fixed flexure was ultimately chosen due to: 1) potential for high discrepancy in moments of inertia between its primary dimensions, 2) approximately linear dynamics assuming fixed bolted connections and relatively small displacements, and

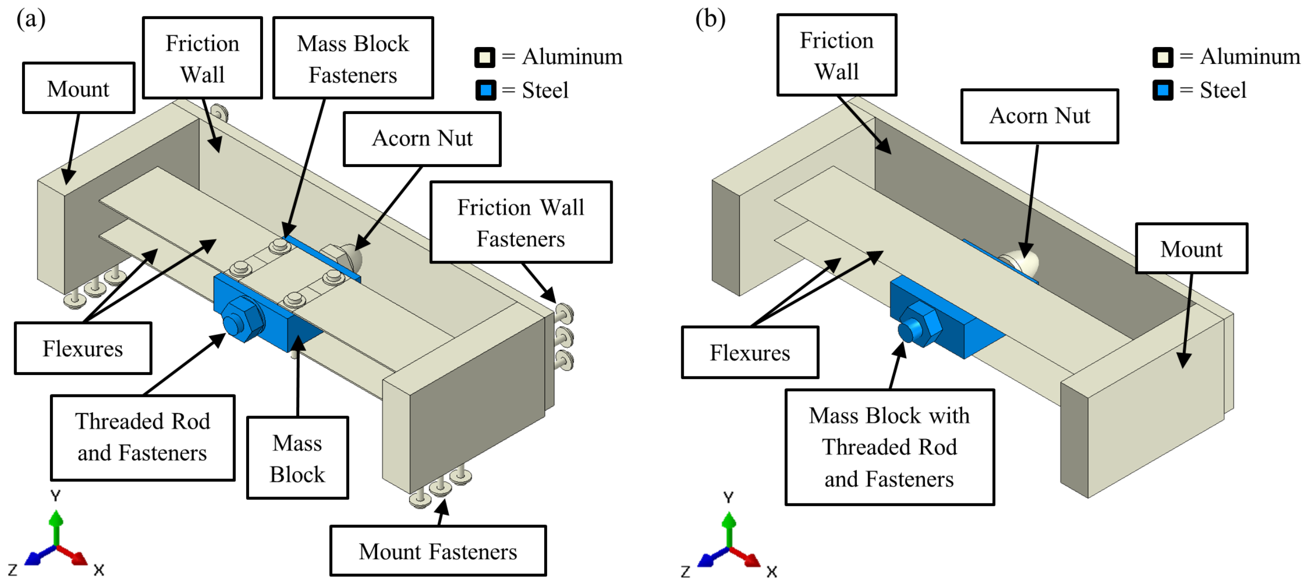

Fig. 8 (a) Detailed model and (b) defeatured model of TVA design.

3) relative manufacturing ease. Additionally, a fixed-fixed flexure, along with the threaded rod, eliminates any reliance on gravity to induce a normal load for a friction contact and can minimize any gravitational effects with well-chosen moments of inertia. This allows the TVA to be oriented in different directions, a need clearly demonstrated by the directional study in the SDoF TVA Directional Analysis section (see Fig. 7). Originally, the TVA was designed as a single flexure with a mass in the center. However, the single flexure design saw undesired torsional modes that were too easily excited; the solution to this issue is discussed below.

Next, the friction contact was considered. Initial design concepts included friction contact with the surface of the BA itself, but this would prove difficult in controlling the normal force while also potentially being an undesired source of wear on the host structure. Instead, the TVA was designed to include a built-in "friction wall" (see Fig. 8) to serve as the contact surface for nonlinear energy dissipation, making the friction contact surfaces independent of the host structure attachment. Degradation of the TVA is preferable to damage of the host structure, as oftentimes replacing the TVA is much less costly than repairing or replacing the host structure. Furthermore, the nature of the contact required careful handling in terms of simulation and practical considerations; the options lied between emulating surface-to-surface contact or point-to-surface contact (edge-to-surface contact, though plausible, was not considered in this design). Surface-to-surface contact emulation (e.g., a flat face rubbing on the friction wall) came with the benefit of providing a counteracting moment force (between the mass and friction wall) to prevent the excitation of torsional modes. However, it is this reactionary moment that raised a concern of uneven pressure distribution at the point of contact. Furthermore, true surface-to-surface contact is often not realized in practice due to inherent variabilities in the contact surfaces. To mitigate this issue, a second fixed-fixed flexure of equal length and thickness was introduced similar to that presented in [23]. This had the effect of greatly increasing the torsional stiffness to minimize the potential for undesired torsional oscillation. From here, the design settled on a point-to-surface contact which was emulated through contact between a rounded end and the friction wall. For the rounded end, several configurations were considered, including a carriage bolt head (like in Lupini et al. [5]), a round-end ball screw, and acorn nut attached to a threaded rod. All of these components are readily available for purchase from retail providers, an important aspect for minimizing manufacturing costs. The acorn nut and threaded rod were ultimately chosen due to their tunability and repairability with respect to both linear and nonlinear system properties.

The last consideration in the design process was the tunability of the TVA. This refers to the ease in which the TVA parameters can be adjusted to affect its target natural frequency and response amplitude. For the TVA in Fig. 8, the main factors affecting the natural frequency are the flexure stiffness, mass properties, and geometry. The factors affecting the frictional force are the normal force applied at the point of contact and the friction coefficient between the surfaces. Designing the TVA to include adjustable flexure stiffness was deemed impractical. Instead, the flexures' length and thickness were chosen to result in a TVA natural frequency that was reasonably close to the target mode; these parameters remained constant. Additionally, the threaded rod comes with the capability to thread on additional mass at the end not in contact with the friction wall, as well as allow for an adjustable applied normal force. Lastly, the acorn nut is not only replaceable, but its material can be changed to modify the friction coefficient between itself and the friction wall. Were this design to be used in practice, it is recommended that that the acorn nut be the softer of the two materials so that it experiences the majority of the wear, as an acorn nut is more easily replaced.

Another important aspect of the TVA is its mass distribution, namely between the "oscillating mass" and the "dead mass" (see Fig. 9). The term "dead mass" is used to define the mass of the TVA which is not contributing to energy dissipation and primarily moves as a rigid body with the host structure. The dead mass typically consists of the hardware used to attach the TVA to the host, though in this study also includes the friction wall and mounts. The mounts consist of blocks with enough bending stiffness to act as fixed ends for the flexures, and in a physical realization of the TVA would be bolted to the host structure. Conversely, oscillating mass is mass whose motion is caused by absorption of energy from the host. Together these two masses make up the total mass of the TVA.

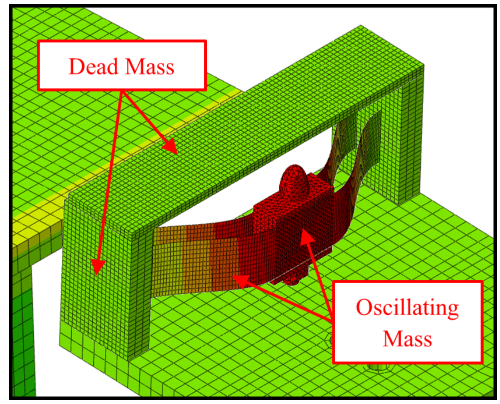

Fig. 9 "Dead mass" vs. "oscillating mass".

This design can be analytically approximated as two fixed-fixed beams acting in parallel. Being able to predict the natural frequency of one's TVA is important in expediting the design process and verifying computational results. The analytical approximation of this TVA's fundamental frequency f_1, while not exact due to assumptions and simplifications needed for analytical formulation, is given in Eq. (12) as:

$$f_1 = \frac{1}{2\pi}\sqrt{\frac{384EI}{L^3 m}} \tag{12}$$

with E, I, and L referring to Young's modulus, area moment of inertia (for configuration shown in Fig. 9, about axis in same direction as the global y-axis), and length (not including the portion attached to the oscillating block) of a single flexure, respectively, and m referring to the mass of the oscillating block. Using parameter values from one of the studied TVA configurations (e.g., $E = 69\times10^9$ Pa, $I = 1.56\times10^{-14}$ m^4, $L = 0.05$ m, and $m = 0.0115$ kg), Eq. (12) gives an estimated frequency of 85.34 Hz. The derivation of Eq. (12) is provided in the Appendix. For designs that closely resemble simple beam structures with or without attachments that approximate point masses, analogous analytical equations are recommended to be used initially to provide estimates informing configuration feasibility and design parameters.

As mentioned previously, the design process was iterative. While the goal was to create a TVA that was applicable to the BA, the design process was also intended to include steps that could be applied more generally for TVA design. Important considerations realized throughout the process are noted and discussed in the Discussion section.

Combined BA-TVA Systems and TVA Tuning

Once the TVA design was satisfactory, five separate FE models of BA-TVA systems (henceforth referred to as "combined systems") were created. In each model, the TVA was mounted at one of the five locations of interest (corresponding to the five nodes in Fig. 6). Figure 10 shows the five FE models, illustrating the five TVA attachment locations.

Initial linear simulations of the combined-system ROMs showed that the TVA split the resonant frequency into an upper peak and a lower peak, as is expected of a well-designed TVA [1]. However, the TVA's effectiveness varies with the tuning of the linear parameters, and thus an optimal tuning had to be found for each attachment location. "Optimal tuning" varies greatly by application; some designers may value how far the new FRF peaks are moved from the original resonance, while others might place greater weight on amplitude reduction.

For this study, two metrics were defined to quantify the performance of the TVA. The first metric, called Peak Split Factor (PSF), quantifies how symmetrically split the two peaks are around the original natural frequency. PSF is defined as:

$$\text{PSF} = \frac{\omega_0 - \omega_{lower}}{\omega_{upper} - \omega_{lower}} \tag{13}$$

where ω_0 is the original target natural frequency of the BA alone, and ω_{upper} and ω_{lower} refer to the combined system's upper and lower natural frequencies, respectively. A PSF value can range from 0 to 1, where a value of 0.5 indicates a perfectly symmetric split. Values lower than 0.5 indicate that the lower peak is closer to the original resonance than the upper peak, and values higher than 0.5 indicate the opposite. Values out of this 0 to 1 range indicate that both peaks are either above or below the original target resonant frequency, making the metric inapplicable. For some applications, it is desirable to have the two peaks as far from the target resonance as possible (i.e., equidistant from the target resonance). For

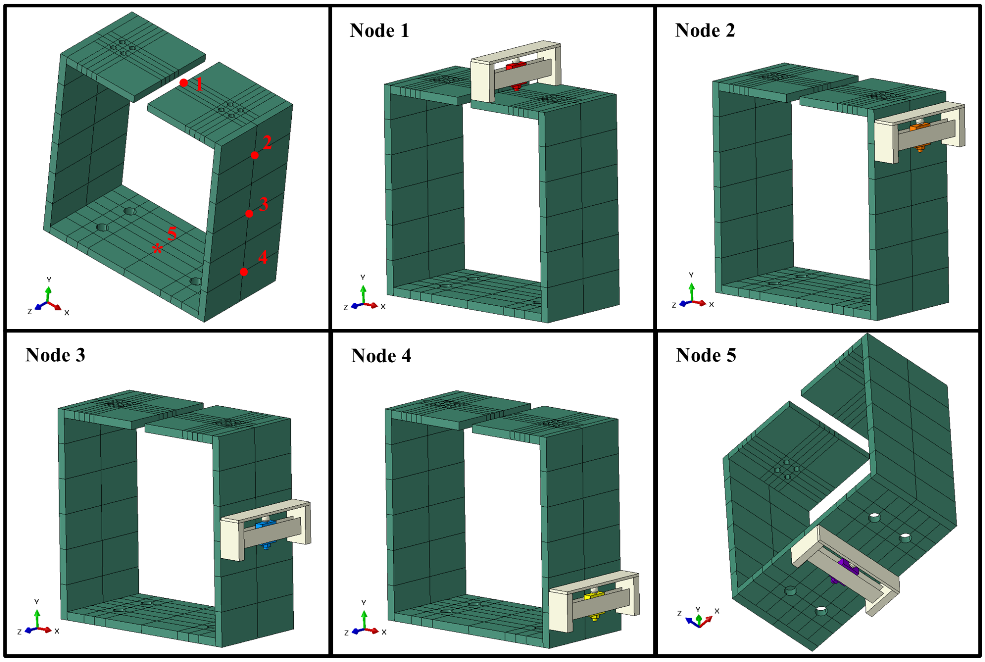

Fig. 10 From top left – BA model with five nodes of interest (* indicates node on backside relative to view shown), the combined model with the TVA at nodes 1 and 2. From bottom left – the combined models with the TVA at nodes 3, 4, and 5. Different colored TVA mass blocks represent different material densities.

example, consider a scenario where the operational environment is predicted to induce a narrowband harmonic forcing with a frequency of ± 1.0 Hz around a host structure's original natural frequency, and a TVA can create a maximum of a 3.0 Hz split between the new natural frequencies. In this case, an effective peak split would result in the new natural frequencies being symmetrically spaced to provide a 0.5 Hz tolerance on both sides of the forcing frequency band. In this example, a symmetric split leads to the lowest risk of resonating at the new natural frequencies.

In this study, it was initially assumed that an optimally tuned TVA was one which prioritized PSF. For this work, if a PSF value between 0.45 and 0.55 could be achieved, the TVA designed was considered tuned for that specific placement location. As will be discussed in the Results section, this tuning scheme was found to be adequate when the TVA was placed at nodes 1, 2, and 3 (i.e., low LRs). However, this was not the case for nodes 4 and 5 (i.e., high LRs). For an application where the applied harmonic forcing has a frequency band greater than the split achievable by the TVA, the host structure could still resonate at one of the new natural frequencies, potentially damaging the structure. As a result, a second tuning iteration was conducted for nodes 4 and 5 using a new performance metric, called Peak Reduction (PR). PR is defined as:

$$\mathrm{PR} = \frac{\max\left(Y_0\left(\omega\right)\right) \ - \max\left(Y\left(\omega\right)\right)}{\max\left(Y_0\left(\omega\right)\right)} \cdot 100 \tag{14}$$

where $\max\left(Y_0\left(\omega\right)\right)$ is the maximum response amplitude of the BA alone and $\max\left(Y\left(\omega\right)\right)$ the maximum response amplitude of the combined system, both over the entire frequency range of interest. PR quantifies the response amplitude reduction due to the addition of the linear TVA, regardless of the shift in natural frequencies of the new resonant peaks. Higher values of PR correspond to greater amplitude reductions for the host structure, and therefore indicate greater TVA effectiveness. A PR greater than 45% was considered adequate for this tuning iteration.

As mentioned previously, linear tuning of this TVA design is achieved through the addition of mass. In practice, this would be achieved be screwing an additional mass onto the end of the threaded rod going through the oscillating mass. For simulation purposes, the density of the mass in the TVA model was adjusted to emulate this additional (or detracted) mass, rather than adding new geometry to the model. This allowed for mesh consistency across all simulations while performing linear tuning iterations, in addition to avoiding: 1) potential computational discrepancies due to mesh regeneration, and 2) time needed for remeshing. Table 1 shows the mass densities of the oscillating mass used at each considered node/attachment location for both tuning iterations along with their resulting PSF and PR values.

In total, seven combined system FE models were created (five tuned for PSF, and two tuned for PR considering node 4 and 5 attachment locations specifically), and CC-CMS reduced-order mass and stiffness matrices were extracted for each model.

Table 1 Densities of oscillating mass and equivalent added mass after tuning the TVA for each node/attachment location, with resulting PSF and PR values.

Target Tuning Metric	Node	Density of Oscillating Mass, [kg/m^3]	Equivalent Added Mass, [%]	Resulting PSF	Resulting PR, [%]
PSF	1	7800*	–	0.477	51.4
	2	8000	2.3	0.452	50.2
	3	8400	6.9	0.456	53.1
	4	8860	12.2	0.487	20.2
	5	9000	13.8	0.458	3.8
PR	4	8400	6.9	0.033	50.8
	5	8220	4.8	–	48.8

*Nominal steel density

For each ROM, three master nodes (i.e., 9 retained master DoFs) were retained: 1) a response node, which is coincident with node 1, and 2) a contact pair of nodes – one on the friction wall and one on the tip of the acorn nut. Because the harmonic forcing was applied at the response node in the x-direction (see Fig. 6) for all cases, this minimal set of retained nodes allows for: 1) applying the external harmonic force and nonlinear forces directly in the reduced-order space, and 2) calculating desired responses without necessitating a projection back to the full-order system coordinates. All linear and nonlinear MATLAB simulations of the combined systems presented in the Results section considered these reduced-order matrices for the respective TVA attachment locations and tunings indicated.

Results

Linear Simulations

Linear simulations of the combined systems were performed using each of the seven ROMs, and the resulting FRFs are shown in Fig. 11 along with the FRF of the BA alone (i.e., no TVA) for comparison. As with the SDoF TVA simulations, the harmonic excitation was applied in the x-direction at node 1, and the presented FRFs are for the x-DoF at node 1.

With the linear TVA tuned with respect to PSF, a nearly even split is seen for all five nodes. As the LR increases from node 1 to node 5, the resulting natural frequencies converge toward that of the BA alone with no TVA, though the two resulting peaks remain approximately equidistant from the original resonance. For the cases with a TVA attached at nodes 1, 2, and 3, a PR above 50% is achieved. However, for the cases with a TVA attached at nodes 4 and 5 and PSF-based tuning, peak magnitudes are similar to that of the BA alone, having PRs of 20.2% and 3.8%, respectively. When the TVAs for these placements were retuned with respect to PR, their resulting FRF peaks were reduced yielding PR values above 48%. However, their respective PSF values after tuning for PR shifted out of the desired range (0.45 – 0.55) as shown in Table 1. Because both resulting natural frequencies of the combined system with the TVA placed at node 5 were above the original target natural frequency ω_0, the PSF was not applicable and is thus not reported in Table 1. This phenomenon is discussed further in the Design Considerations section.

Nonlinear Simulations

The same reduced-order matrices used for linear simulations were also used for all nonlinear simulations, with friction contact now included between the contact pair DoFs. For all presented nonlinear simulations, the same harmonic excitation and response DoF as that used for linear simulations is considered. Time series simulations were computed using Eq. (10) and ode45 in MATLAB for individual excitation frequencies within the frequency range of interest. Steady-state response amplitudes (peak-to-peak amplitude divided by 2) were calculated for each excitation frequency once response amplitudes were no longer changing in time, and the results compiled to produce a nonlinear FRF.

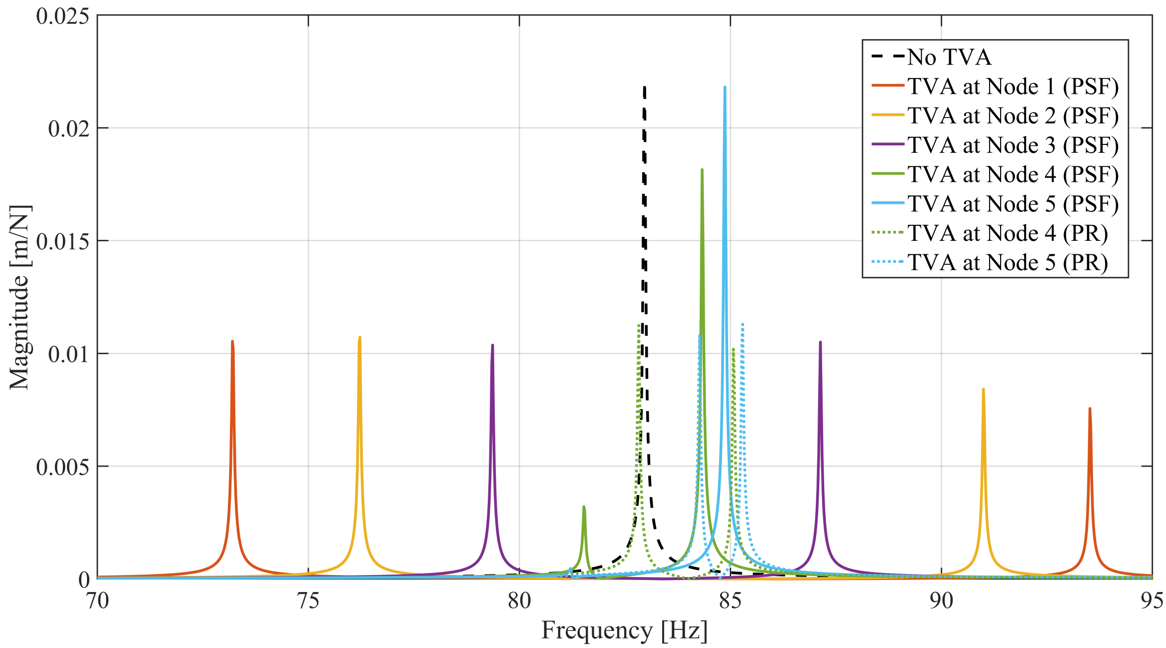

Fig. 11 Linear FRFs of the BA alone and combined systems with TVA attached at the five nodes of interest. PSF-based tunings are shown for attachment at nodes 1, 2, and 3, and both PSF-based and PR-based tunings are shown for attachment at nodes 4 and 5.

From linear simulations, the highest achievable peak reduction across all attachment locations was 48.8%; with the addition of friction, the goal was to attain over 90% PR for each TVA attachment location. Thus, the PR-based TVA tuning was considered for nonlinear simulations with the TVA attached at nodes 4 and 5. However, as mentioned previously, PSF-based TVA tuning with the TVA attached at nodes 1, 2, and 3 was sufficient, and thus the PSF-tuned versions of the TVA were maintained. Nonlinear simulations consisted of varying the value of the dimensionless microslip parameter $\mu N/F$,

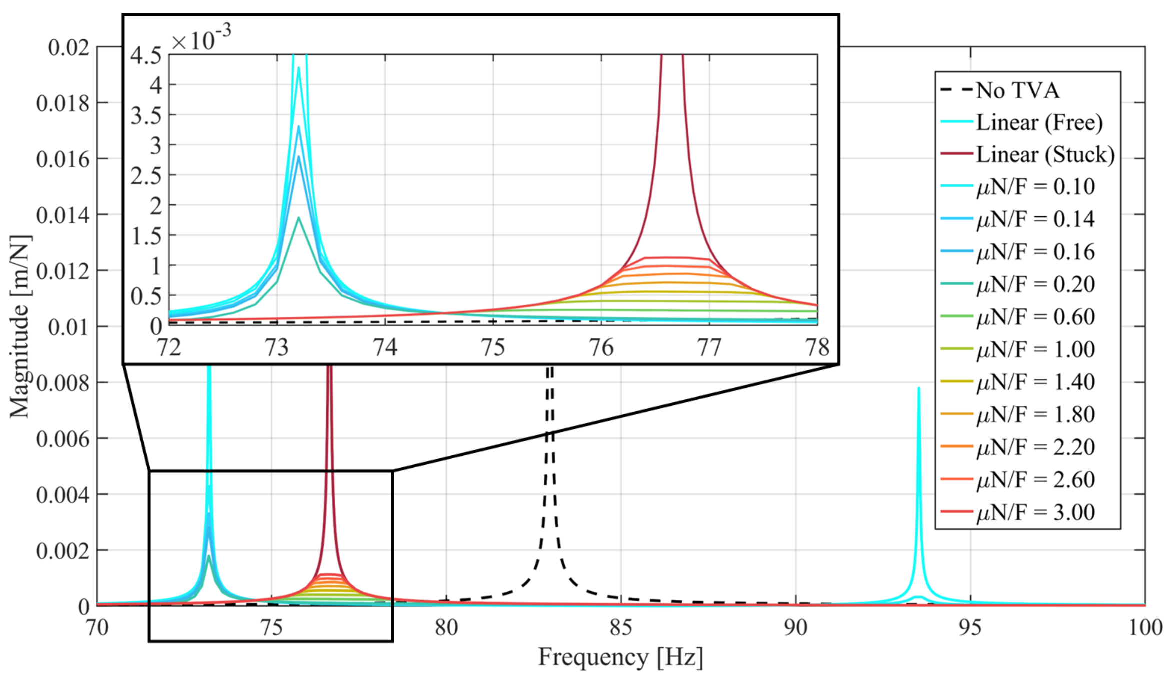

Fig. 12 Nonlinear FRFs for friction-enhanced TVA attached at node 1.

i.e., the ratio of the friction force, μN, to the external forcing amplitude F. For the systems considered here, note that any combinations of μ, N, and F that yield an identical $\mu N/F$ will yield the same nonlinear response, regardless of the specific values of μ, N, and F considered.

Figure 12 shows nonlinear FRFs considering a range of $\mu N/F$ values for the TVA placed at node 1, and includes the linear FRFs of the "No TVA" and linear TVA (labeled "Linear (Free)") shown in Fig. 11 for reference. Figure 12 also includes the linear "stuck" case (labeled "Linear (Stuck)"), in which $\mu N/F$ is increased to the point of having no relative motion between the contact pair (i.e., the entire TVA acts as dead mass). For this TVA placement, a $\mu N/F$ value of 0.30 attains the maximum PR of 99%.

The focus of this study, however, is the effectiveness of the TVA at high-LR areas, i.e., nodes 4 and 5. TVAs placed at nodes 2 and 3, being low-LR areas, yielded similar results to those presented for the TVA at node 1 and are therefore

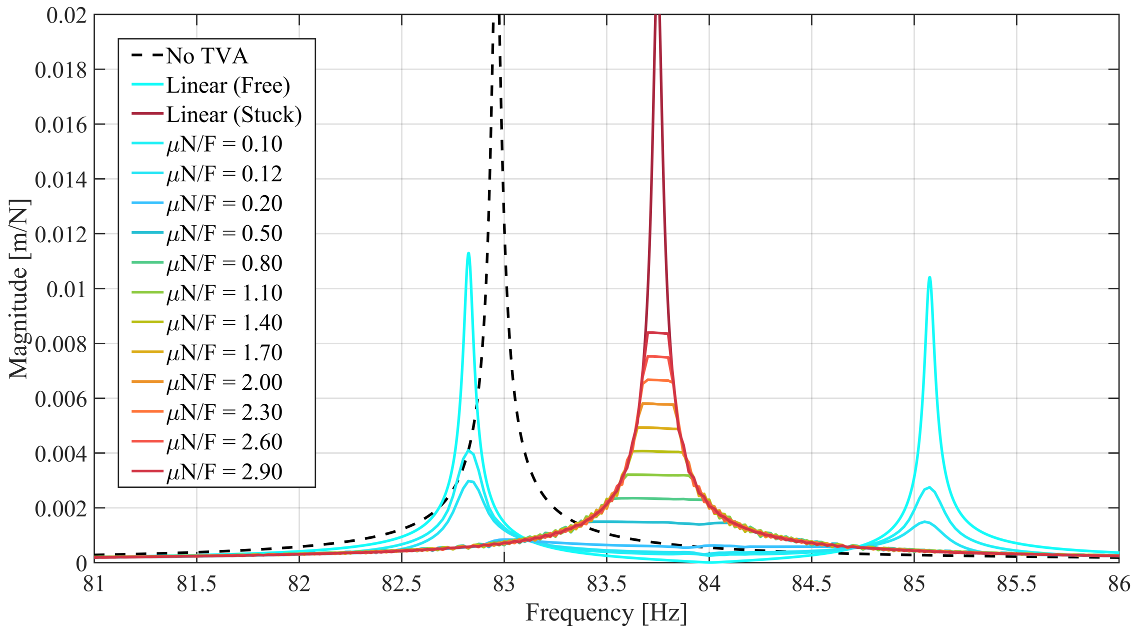

Fig. 13 Nonlinear FRFs for friction-enhanced TVA attached at node 4.

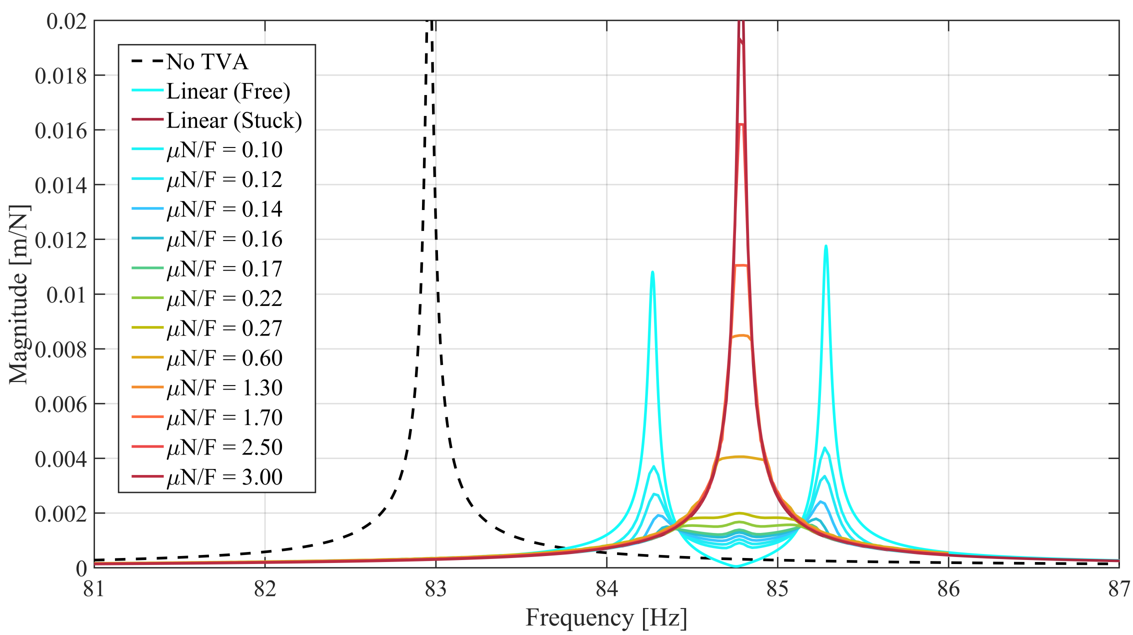

Fig. 14 Nonlinear FRFs for friction-enhanced TVA attached at node 5.

not shown. The nonlinear and reference linear FRFs for TVA placement at nodes 4 and 5 are shown in Figs. 13 and 14, respectively.

When the TVA is placed at node 4, a maximum PR of 96.3% is achieved across all $\mu N/F$ values. When placed at node 5, a maximum PR of 93.3% is achieved. These PR values are achieved for $\mu N/F = 0.20$ and $\mu N/F = 0.18$, respectively.

Discussion

The linear FRFs in Fig. 11 illustrate important trends as the LR increases. For TVA attachment at nodes 1, 2, and 3 with low LRs, tuning for either PSF or PR achieves similar results; however, this is not the case for attachment at nodes 4 and 5 with high LRs. For these TVA attachment locations, there is a dramatic tradeoff between PSF and PR, emphasizing that TVAs attached at high-LR areas can be much more sensitive to tuning than if attached at low-LRs areas. Choosing the optimal tuning scheme is an engineering decision informed by the operational environment and host structure limits.

The nonlinear FRFs considering a friction-enhanced TVA in Figs. 12 – 14 show a dramatic increase in reduction for all attachment locations compared to their respective linear FRFs. For the case of TVA attachment at node 1 (Fig. 12), the nonlinear maximum PR is 99.0%, a vast improvement over that of the linear TVA (51.4%) and comfortably above the desired PR of at least 90%. Similar improvements from 50.8% to 96.3% PR for attachment at node 4 (Fig. 13) and 48.8% to 93.3% PR for attachment at node 5 (Fig. 14) are also achieved. In each case, as $\mu N/F$ increases, the response of the BA begins to leave the linear free FRF and converge to the linear stuck FRF. A trend seen for all TVA placement locations was that the maximum achievable PR tends to occur when the maximum nonlinear response lies at the intersection between the free and stuck curves. This effect agrees with what has been observed in other studies, such as that by Cimpuieru et al. [3].

Figure 15 shows the maximum PR achieved with and without friction for the PR and PSF tuning schemes, with the five data points in each curve corresponding to the five TVA placements considered. For values including friction, the plotted PR values correspond to the greatest PRs achieved for each TVA placement across all simulated $\mu N/F$ values. Without friction, the greatest PR achieved across all five placements is 53.2%. By adding friction, a PR greater than 93% was achieved even at the high-LR placements. As stated previously, this was achieved for PSF-based TVA tuning for placements at nodes 1, 2 and 3, and PR-based TVA tuning for placements at nodes 4 and 5. Figure 15 shows: 1) the improved TVA performance when including friction, 2) the tradeoff between PSF-based and PR-based tuning at high LRs, and 3) that effective vibration reduction is achievable when friction contact is introduced, even for high-LR TVA placements.

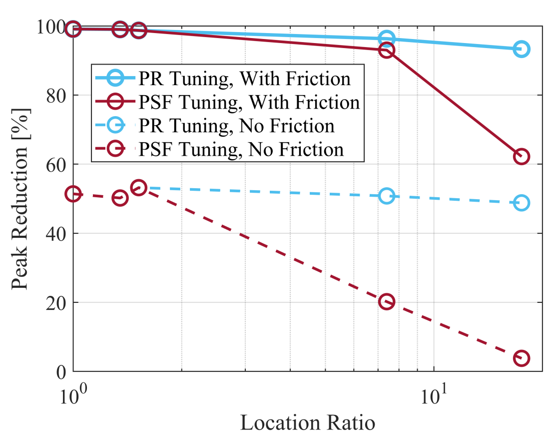

Fig. 15 Peak reduction vs. location ratio for varying TVA placement and tuning scheme.

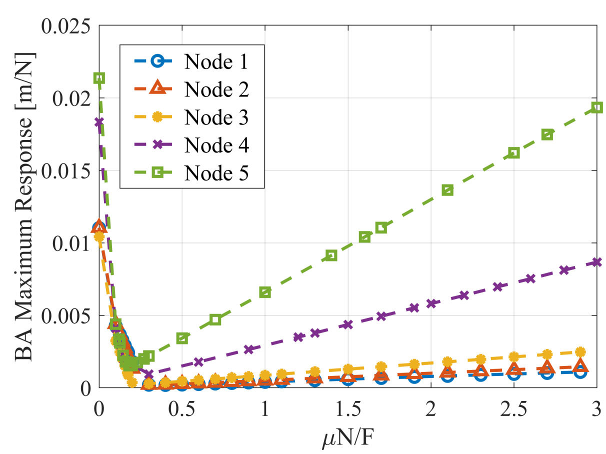

Fig. 16 BA maximum response vs. μN/F for TVA placement at nodes 1 through 5.

Figure 16 displays the BA maximum response for each considered TVA placement location as a function of $\mu N/F$. One can notice that the curves flatten as the TVA placement moves from node 5 to node 1 (i.e., as the LR decreases). That is, for TVA placements at low LRs, there is a significantly larger range of $\mu N/F$ values that achieve a nearly identical reduction as the $\mu N/F$ yielding the greatest reduction. This shows that, while dramatic amplitude response reduction is possible across all LRs, friction contact parameters require more careful tuning to achieve a near-optimal reduction for high-LR TVA placement. In addition, the optimal $\mu N/F$ varies slightly across all TVA placement locations, indicating that the optimal $\mu N/F$ can depend on LR. These results highlight the importance of having a tunable friction contact, as in practice, some iteration is likely needed to achieve optimal, or near optimal, reduction for TVAs placed in a high-LR area.

Design Considerations

Thus far, the presented results have shown agreement with what similar studies in literature have demonstrated – that effective friction-enhanced TVAs can be designed for high-LR applications. However, the design process described here has yielded a number of insights into the nature of friction-enhanced TVA design, which could be used to guide future efforts. These insights have been compiled into the following set of design considerations, with the hope that they will help inform future TVA design efforts and assist in making strategic design choices.

1. Determine potential TVA attachment locations and evaluate feasibility through a location ratio study.
For the host structure considered in this work, it is relatively easy to see where preferable (low-LR) TVA attachment locations exist for the targeted mode through visual examination of the mode shape for mode 1. However, this is may not true for complex structures, and an examination of the displacement amplitudes across the host structure may reveal unexpected variations in LR. After an initial computational modal analysis of the BA, it was found that for some mode/node combinations, the LR was extremely high. For example, the LR at node 5 for mode 2 is approximately 12,751, indicating an almost negligible vibration amplitude at this location. Although mode 2 was not considered in this study, it is reasonable to assume that if a TVA were placed at this location to target mode 2, there would not be enough energy transfer for a TVA to have a significant impact on the BA's response. It is therefore recommended that designers calculate the LR to determine feasible/desirable attachment locations on the host structure for their mode of interest. Doing so allows one to eliminate impractical attachment locations where a TVA would not be able to effectively absorb energy from the host structure.

2. Perform a directional study to determine effective TVA oscillation directions.
The effectiveness of a TVA can vary greatly depending on the direction of oscillation of the TVA mass. In this study, the SDoF TVA directional analyses showed that when targeting mode 1, in most cases, the greatest amplitude reduction was achieved when the TVA mass oscillated in the x-direction (except at node 5), and rarely had any effect when oscillating in the z-direction. Furthermore, a TVA's effectiveness with respect to oscillation direction will differ based on the targeted mode. For the BA, modes 2 and 4 have mode shapes which involve motion in the z-direction, whereas mode 1 did not (see Fig. 17). Therefore, when targeting modes 2 or 4, a TVA oscillating in the z-direction may be more effective.

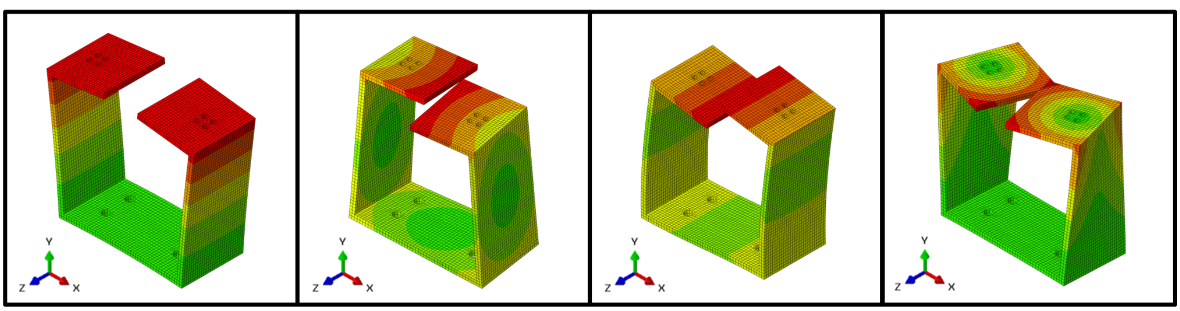

Fig. 17 From left to right, modes 1 through 4 of the BA. The green to red color gradient represents the minimum to maximum displacement gradient, respectively.

For some structures, the choice of oscillation direction is intuitive; if the structure itself oscillates primarily in one direction, that same direction will likely be the optimal choice for the TVA mass' oscillation. This was the case for the BA, where the mode shape associated with mode 1 clearly shows the largest displacement in the x-direction. Consequently, x-direction oscillators were almost always the most effective in this case. However, more complicated host structures may have mode shapes with no obvious primary direction of displacement. Furthermore, there may be oscillation directions that would be preferred, but are not feasible due to geometry or other placement constraints. In these instances, a thorough study of the effectiveness of various oscillation directions is recommended to ensure sufficient energy transfer from the host structure to the TVA.

3. Evaluate the effect of mass loading on the host structure.
In this study, it was found that increasing the amount of dead mass (for the same placement location) decreased the natural frequency of the combined system when the TVA acts a rigidly attached mass (e.g., see linear "stuck" and "No TVA" curves in Fig. 12). For the TVA presented in this work, targeting a lower natural frequency meant increasing the oscillating mass

(see Eq. 12). As such, as the dead mass was increased, the oscillating mass was also increased to compensate for the resulting change in target frequency due to this mass loading effect. Because a heavier TVA is often undesirable for many applications, such as for aerospace structures where mass is typically sought to be minimized, it follows that designers should understand the mass properties of their TVAs and seek to minimize, or utilize, dead mass where possible, and if necessary, account for potential mass loading effects on overall system dynamics.

4. Account for stiffening effects in combined system dynamics due to TVA mounts.
For the high-LR areas in this study (i.e., at nodes 4 and 5), the addition of the TVA increased the combined system natural frequency when the TVA acts as a rigidly attached mass (e.g., see the linear "stuck" and "No TVA" curves in Figs.13 and 14). This is a counterintuitive result, as adding mass is often expected to decrease natural frequency as discussed in design consideration 3. The increase seen for TVA placement at nodes 4 and 5 is due to a stiffening effect caused by the TVA's mounting mechanism as illustrated in Fig. 18.

Considering the area moment of inertia equation for a beam with a rectangular cross-section, $I = bh^3/12$, the BA's area moment of inertia about its bending axis for mode 1 is significantly increased with the introduction of the TVA's mounts. This stiffening effect dominates in comparison to the mass loading effect at high LRs, leading to an overall increase in the combined system's natural frequencies. It follows that designers should understand the stiffening effects of their TVAs and seek to minimize, or utilize, the impact of their mounting mechanisms.

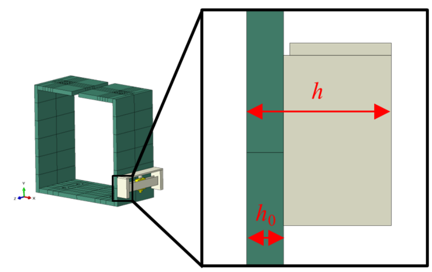

Fig. 18 Structure thickness with, h, and without, h_0, TVA mounts, illustrating effective increase in thickness due to TVA mounts (attachment at node 4 shown).

5. Ensure the TVA is tunable with respect to target natural frequency and friction contact parameters.
TVAs that use friction-based energy dissipation mechanisms are sensitive to many factors, some of which are addressed in this study (i.e., TVA placement, mass, friction coefficient, and normal force). As shown, this is especially true for placements at locations with high LRs (e.g., see Fig. 16). Designing a TVA such that one can adjust these properties based on empirical effectiveness is desirable when optimizing for a selected performance metric. In the case of the presented TVA design, tunability also came with the benefit of repairability due to the replaceable acorn nut. This allows for greater longevity of the overall component. Tunability was achieved in this study via the features portrayed in Fig. 19.

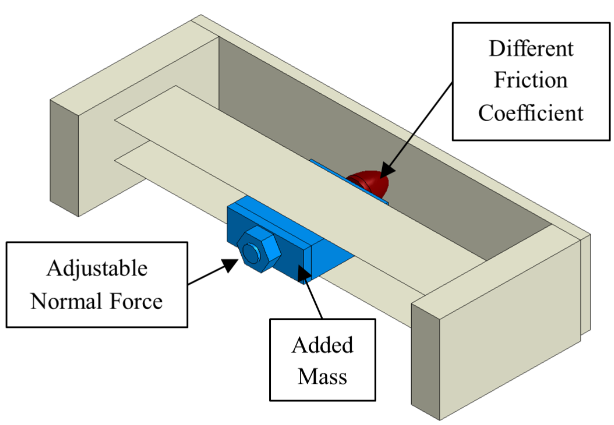

Fig. 19 Tunable features of presented TVA.

6. Tune with respect to the performance metric that best applies to the host structure's operational environment.
Operational environments that can vary dramatically will significantly impact TVA behavior and effectiveness. Understanding the nature of the loads the host structure will experience is crucial to optimizing a TVA's performance. There are several considerations in choosing the best suited performance metric, whether it be from those detailed in this study or one of the designers' choosing. Examples of considerations include, but are not limited to, variety in environmental loading conditions, load frequency band, frequency sweeps encountered during startups and shutdowns, and desired level of vibration absorp-

tion, among others. It is recommended that a metric tailored to the operational environment be chosen, and that the TVA is iteratively tuned as needed to achieve optimal performance.

7. Perform a fatigue analysis to evaluate TVA lifespan within a given operational environment.
Though not shown in this study for brevity, a fatigue analysis is a crucial step that should be performed prior to manufacturing a TVA. An understanding of the anticipated stresses experienced by a TVA during operation will aid designers in predicting the TVA's longevity and scheduling routine repairs/replacement of the TVA or its components.

Future Work

While this study did not consider a physical realization of the TVA, the manufacturing of this TVA would likely reveal insights that could justify (or call into question) the design choices made in this study, and thus give rise to new design considerations. Furthermore, experimental testing of this TVA design would be necessary to corroborate the simulation results and confirm the effectiveness of the TVA. Both steps – the building and testing of the proposed TVA – would further authenticate and inform any augmentations to the design considerations proposed herein.

Acknowledgments This research was funded by Los Alamos National Laboratory (LANL) through the Engineering Institute's Los Alamos Dynamics Summer School. The Engineering Institute is a research and education collaboration between LANL and the University of California San Diego's Jacobs School of Engineering. This collaboration seeks to promote multidisciplinary engineering research that develops and integrates advanced predictive modeling, novel sensing systems, and new developments in information technology to address LANL mission relevant problems. The authors would also like to acknowledge Samantha Ceballes and Julian Davis for contributing their technical expertise to the development of this project.

References

1. Connor, J.J.: Tuned Mass Dampers. In: Introduction to Structural Motion Control. New York, NY, USA. Prentice Hall Pearson Education, Inc., (2003).
2. Sun, J.Q., Jolly, M.R., Norris, M.A.: Passive, Adaptive and Active Tuned Vibration Absorbers—a Survey. Journal of Mechanical Design. (117)B, 234–242 (1995). https://doi.org/10.1115/1.2836462
3. Cimpuieru, M., Kripfgans, A.D., Kelly, S.T., Epureanu, B.I.: Additive Manufacturing of Resonant Vibration Absorbers for Turbomachinery Blisks. Presented at the IMAC XLII, Orlando, Florida, USA, (2024).
4. Lupini, A., Mitra, M., Epureanu, B.I.: Application of Tuned Vibration Absorber Concept to Blisk Ring Dampers: A Nonlinear Study. Journal of Engineering for Gas Turbines and Power. (141)10, 101016 (2019). https://doi.org/10.1115/1.4044684
5. Lupini, A., Shim, J., Epureanu, B.I.: Experimental and Computational Study of a Tuned Damper with Frictional Contacts. AIAA Journal. (58)8, 3607–3613 (2020). https://doi.org/10.2514/1.J059393
6. Dalisay, J.D.E., Moore, K.J., Bergman, L.A., Vakakis, A.F.: Local Nonlinear Stores Induce Global Modal Interactions in the Steady-State Dynamics of a Model Airplane. Journal of Sound and Vibration. (500), 116020 (2021). https://doi.org/10.1016/j.jsv.2021.116020
7. Aksoy, T., Acar, B., Özgen, G.O.: A Novel Method for the Vibration Reduction of an Air Vehicle Missile Launcher. In: AIAA Scitech 2019 Forum. https://doi.org/10.2514/6.2019-0494
8. Cimpuieru, M., Kelly, S.T., Epureanu, B.I.: Computational Analysis of Tuned Vibration Absorbers with Impact and Friction Contacts. In: AIAA Scitech 2023 Forum. https://doi.org/10.2514/6.2023-2075
9. Cimpuieru, M., Kelly, S.T., Epureanu, B.I.: Resonant Vibration Absorbers with Impacts. In: Nonlinear Structures & Systems, Volume 1, Conference Proceedings of the Society for Experimental Mechanics Series. 237–241 (2023). https://doi.org/10.1007/978-3-031-36999-5_31
10. Nasr, A., Mrad, C., Nasri, R.: A Study of Friction Vibration Absorber: Impact of Friction Modeling on the Efficacy of the Absorber and Friction Coefficient Optimization. Mechanics & Industry. (19)6, (2018). https://doi.org/10.1051/meca/2018039
11. Pisal, A.Y., Jangid, R.S.: Dynamic Response of Structure with Tuned Mass Friction Damper. International journal of Advanced Structural Engineering. (8)4, 363–377 (2016). https://doi.org/10.1007/s40091-016-0136-7
12. Wang, C., Brown, J.D., Singh, A., Moore, K.J.: A Two-Dimensional Nonlinear Vibration Absorber Using Elliptical Impacts and Sliding. Mechanical Systems and Signal Processing. (189), 110068 (2023). https://doi.org/10.1016/j.ymssp.2022.110068
13. Wang, Y., Ma, Y., Wang, H., Firrone, C.M., Hong, J.: Dynamic Performance of a Novel Tuned Vibration Absorber with Nonlinear Friction Interfaces. Nonlinear Dynamics. (112)11, 8831–8848 (2024). https://doi.org/10.1007/s11071-024-09347-8
14. Hong, H.K., Liu, C.S.: Coulomb Friction Oscillator: Modelling and Responses to Harmonic Loads and Base Excitations. Journal of Sound and Vibration. (229)5, 1171–1192 (2000). https://doi.org/10.1006/jsvi.1999.2594
15. Wang, X., Wang, R., Huang, B., Mo, J., Ouyang, H.: A Study of Effect of Various Normal Force Loading Forms on Frictional Stick-Slip Vibration. Journal of Dynamics, Monitoring and Diagnostics. (1)1, 46–55 (2021). https://doi.org/10.37965/jdmd.v2i2.48
16. Griffin, J.H., Menq, C.-H.: Friction Damping of Circular Motion and Its Implications to Vibration Control. Journal of Vibration and Acoustics. (113)2, 225–229 (1991). https://doi.org/10.1115/1.2930173

17. Mitra, M., Lupini, A., Epureanu, B.I.: A Study on the Application of Tuned Vibration Absorbers to Nominally Cyclic Structures. In: ASME Turbo Expo 2019: Turbomachinery Technical Conference and Exposition, Volume 7B: Structures and Dynamics, V07BT35A002. Pheonix, Arizona, USA (2019). https://doi.org/10.1115/GT2019-90167
18. Lupini, A., Epureanu, B.I.: A Friction-Enhanced Tuned Ring Damper for Bladed Disks. Journal of Engineering for Gas Turbines and Power. (143)1, 011002 (2021). https://doi.org/10.1115/1.4049203
19. Lupini, A.: Computational Models and Damper Concepts for Vibration Reduction of Turbomachinery Blisks. Ph.D. Thesis. University of Michigan. (2020).
20. Craig, R.R., Chang, C.-J.: Free-Interface Methods of Substructure Coupling for Dynamic Analysis. AIAA Journal. (14)11, 1633–1635 (1976). https://doi.org/10.2514/3.7264
21. Krack, M., Gross, J.: Harmonic Balance for Nonlinear Vibration Problems. Springer Cham, (2019). https://doi.org/10.1007/978-3-030-14023-6
22. Hart, K., Lewis, E., Sinclair, S., Moore, K.J., Flynn, G.S., Haynes, C.: A Characterization of the Uncertainty in Force-Control Testing for Aerospace Applications. Presented at the IMAC XLII, Orlando, Florida, USA, (2024).
23. Singh, A., Moore, K.J.: Identification of Multiple Local Nonlinear Attachments Using a Single Measurement Case. Journal of Sound and Vibration. (513), 116410 (2021). https://doi.org/10.1016/j.jsv.2021.116410

Appendix

This section details the step-by-step derivation of the analytical equation, Eq. (12), used to guide this study's initial TVA design efforts. A sketch of a simplified configuration used to model the presented TVA design is given in Fig. A.1.

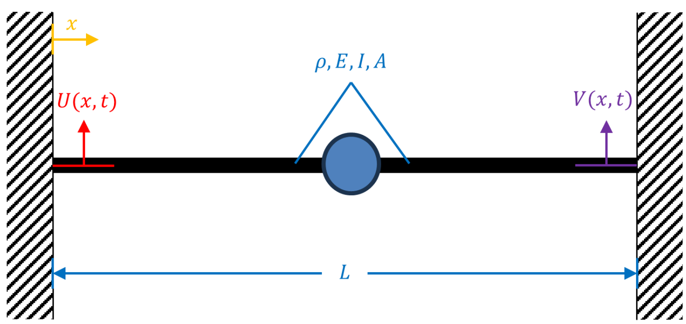

Fig. A.1 Simplified sketch of single flexure with center mass.

The governing equations (considering a local frame) are given by:

$$\rho A U_{tt} + EIU_{xxxx} = 0, \text{ for } 0 \leq x \leq \frac{L}{2} \tag{A.1}$$

$$\rho A V_{tt} + EIV_{xxxx} = 0, \text{ for } \frac{L}{2} \leq x \leq L \tag{A.2}$$

where ρ is the mass density per unit area, A the cross-sectional area, E the Young's modulus, I the area moment of inertia about the out-of-plane axis in Fig. A.1, L the length (not including the portion attached to the oscillating block), m the mass of the oscillating block, and $U(x,t)$ and $V(x,t)$ the respective displacement of the flexures on either side of the oscillating block.

Applying fixed boundary conditions at $x = 0$ and $x = L$ and compatibility conditions at $L/2$ yields the following relations:

$$U(0,t) = U_x(0,t) = 0 \tag{A.3}$$

$$V(L,t) = V_x(L,t) = 0 \tag{A.4}$$

$$U\left(\frac{L}{2},t\right) = V\left(\frac{L}{2},t\right) \tag{A.5}$$

$$U_x\left(\frac{L}{2},t\right) = V_x\left(\frac{L}{2},t\right) \tag{A.6}$$

$$\text{(Assume)}\quad EIU_{xxx}\left(\frac{L}{2},t\right) = P \tag{A.7}$$

$$\text{(Assume)}\quad EIV_{xxx}\left(\frac{L}{2},t\right) = -P \tag{A.8}$$

Considering the static problem (i.e., $U(x)$ and $V(x)$ no longer consider a time dependency) and enforcing defined boundary and compatibility conditions gives:

$$EIU_{xxxx}(x) = 0,\ \text{for}\ 0 \le x \le \frac{L}{2} \tag{A.9}$$

$$EIV_{xxxx}(x) = 0,\ \text{for}\ \frac{L}{2} \le x \le L \tag{A.10}$$

$$U(0) = U_x(0) = 0 \tag{A.11}$$

$$V(L) = V_x(L) = 0 \tag{A.12}$$

$$U\left(\frac{L}{2}\right) = V\left(\frac{L}{2}\right) \tag{A.13}$$

$$U_x\left(\frac{L}{2}\right) = V_x\left(\frac{L}{2}\right) = 0 \tag{A.14}$$

$$\text{(Assume)}\quad EIU_{xxx}\left(\frac{L}{2}\right) = P \tag{A.15}$$

$$\text{(Assume)}\quad EIV_{xxx}\left(\frac{L}{2}\right) = -P \tag{A.16}$$

The solution forms for $U(x)$ and $V(x)$ considering integration constants a, b, c, and d for $U(x)$ and e, f, g, and h for $V(x)$, respectively, are:

$$U(x) = \frac{1}{EI}\left(\frac{1}{6}ax^3 + \frac{1}{2}bx^2 + cx + d\right) \tag{A.17}$$

$$V(x) = \frac{1}{EI}\left(\frac{1}{6}ex^3 + \frac{1}{2}fx^2 + gx + h\right) \tag{A.18}$$

Applying boundary conditions in Eqs. (A.11) and (A.12) for Eqs. (A.17) and (A.18) gives:

$$U(0) \rightarrow d = 0;\ \ U_x(0) \rightarrow c = 0 \tag{A.19}$$

$$V(L) = \frac{1}{EI}\left(\frac{1}{6}eL^3 + \frac{1}{2}fL^2 + gL + h\right) = 0 \tag{A.20}$$

$$V_x(L) = \frac{1}{EI}\left(\frac{1}{2}eL^2 + fL + g\right) = 0 \tag{A.21}$$

Implicitly using Eq. (A.19) and applying the compatibility conditions in Eqs. (A.13), (A.15), and (A.16), respectively, gives:

$$\frac{1}{EI}\left[\frac{1}{6}a\left(\frac{L}{2}\right)^3 + \frac{1}{2}b\left(\frac{L}{2}\right)^2\right] = \frac{1}{EI}\left[\frac{1}{6}e\left(\frac{L}{2}\right)^3 + \frac{1}{2}f\left(\frac{L}{2}\right)^2 + g\left(\frac{L}{2}\right) + h\right] \tag{A.22}$$

$$EIU_{xxx}\left(\frac{L}{2}\right) = a = P \tag{A.23}$$

$$EIV_{xxx}\left(\frac{L}{2}\right) = e = -P \tag{A.24}$$

Similarly, substituting Eqs. (A.17) and (A.18) into Eq. (A.14) respectively gives:

$$U_x\left(\frac{L}{2}\right)=\frac{1}{EI}\left[\frac{1}{2}a\left(\frac{L}{2}\right)^2+b\left(\frac{L}{2}\right)\right]=0 \tag{A.25}$$

$$V_x\left(\frac{L}{2}\right)=\frac{1}{EI}\left[\frac{1}{2}e\left(\frac{L}{2}\right)^2+f\left(\frac{L}{2}\right)+g\right]=0 \tag{A.26}$$

Equations (A.20), (A.21), (A.22), (A.25), (A.26), and (A.23) can be written in matrix form (not including $c=0$ and $d=0$ from Eq. (A.19)) as:

$$\begin{bmatrix} 0 & 0 & \frac{L^3}{6EI} & \frac{L^2}{2EI} & \frac{L}{EI} & \frac{1}{EI} \\ 0 & 0 & \frac{L^2}{2EI} & \frac{L}{EI} & \frac{1}{EI} & 0 \\ \frac{-L^3}{48} & \frac{-L^2}{8} & \frac{L^3}{48} & \frac{L^2}{8} & \frac{L}{2} & 1 \\ \frac{L^2}{8EI} & \frac{L}{2EI} & 0 & 0 & 0 & 0 \\ 0 & 0 & \frac{L^2}{8EI} & \frac{L}{2EI} & \frac{1}{EI} & 0 \\ 1 & 0 & 0 & 0 & 0 & 0 \end{bmatrix}\begin{bmatrix} a \\ b \\ e \\ f \\ g \\ h \end{bmatrix}=\begin{bmatrix} 0 \\ 0 \\ 0 \\ 0 \\ 0 \\ P \end{bmatrix} \tag{A.27}$$

Solving Eq. (A.27) yields the non-zero integration constants:

$$a=P;\ b=\frac{-LP}{4};\ e=-P;\ f=\frac{3LP}{4};\ g=-\frac{L^2P}{4};\ h=\frac{L^3P}{24} \tag{A.28}$$

where a and e are also in agreement with Eqs. (A.23) and (A.24), respectively. Substituting the integration constants in Eqs. (A.19) and (A.28) into Eqs. (A.17) and (A.18) respectively gives:

$$U(x)=\frac{1}{EI}\left(\frac{P}{6}x^3-\frac{LP}{8}x^2\right) \tag{A.29}$$

$$V(x)=\frac{1}{EI}\left(\frac{-P}{6}x^3+\frac{3LP}{8}x^2-\frac{L^2P}{4}x+\frac{L^3P}{24}\right) \tag{A.30}$$

Considering a unit applied load $F=1$ at the mass location $x=L/2$ (corresponding to shear $P=-1/2$) and solving for stiffness $k(x)$ when evaluated at $x=L/2$ yields:

$$k\left(\frac{L}{2}\right)=\frac{F}{U\left(\frac{L}{2}\right)}=\frac{192EI}{L^3} \tag{A.31}$$

One can note that assuming the flexures are massless and completely dictate the TVA stiffness, Eq. (A.31) is equal to the fixed-fixed beam stiffness at the mass location where max deflection occurs. Lastly, using the expression for $k\left(L/2\right)$ in Eq. (A.31) to calculate the structure's fundamental frequency f_1 (not the integration constant f) gives Eq. (A.32) which is equal to Eq. (12):

$$f_1=\frac{1}{2\pi}\sqrt{\frac{2k}{m}}=\frac{1}{2\pi}\sqrt{\frac{384EI}{L^3m}} \tag{A.32}$$

where $k=k\left(L/2\right)$ in Eq. (A.31). Note that because there are two flexures acting in parallel for the actual TVA design, an overall stiffness of $2k$ is considered in Eq. (A.32).